JACS
JOURNAL OF THE AMERICAN CHEMICAL SOCIETY

ARTICLE

pubs.acs.org/JACS

Multiscale Simulation Reveals Multiple Pathways for H_2 and O_2 Transport in a [NiFe]-Hydrogenase

Po-hung Wang,[†] Robert B. Best,[*,‡] and Jochen Blumberger[*,†]

[†]Department of Physics and Astronomy, University College London, London WC1E 6BT, United Kingdom

[‡]Department of Chemistry, University of Cambridge, Lensfield Road, Cambridge CB2 1EW, United Kingdom

Supporting Information

ABSTRACT: Hydrogenases are enzymes that catalyze the reversible conversion of hydrogen molecules to protons and electrons. The mechanism by which the gas molecules reach the active site is important for understanding the function of the enzyme and may play a role in the selectivity for hydrogen over inhibitor molecules. Here, we develop a general multiscale molecular simulation approach for the calculation of diffusion rates and determination of pathways by which substrate or inhibitor gases can reach the protein active site. Combining kinetic data from both equilibrium simulations and enhanced sampling, we construct a master equation describing the movement of gas molecules within the enzyme. We find that the time-dependent gas population of the active site can be fit to the same phenomenological rate law used to interpret experiments, with corresponding diffusion rates in very good agreement with experimental data. However, in contrast to the conventional picture, in which the gases follow a well-defined hydrophobic tunnel, we find that there is a diverse network of accessible pathways by which the gas molecules can reach the active site. The previously identified tunnel accounts for only about 60% of the total flux. Our results suggest that the dramatic decrease in the diffusion rate for mutations involving the residue Val74 could be in part due to the narrowing of the passage Val74−Arg476, immediately adjacent to the binding site, explaining why mutations of Leu122 had only a negligible effect in experiment. Our method is not specific to the [NiFe]-hydrogenase and should be generally applicable to the transport of small molecules in proteins.

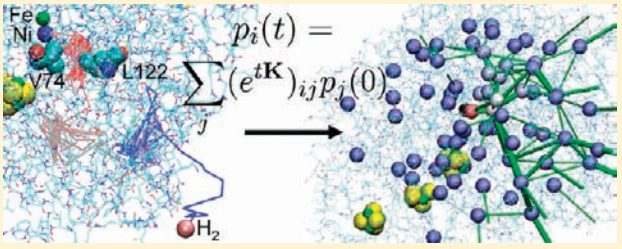

1. INTRODUCTION

Small molecule transport in proteins is an ubiquitous physical process in biochemistry.[1,2] A large number of enzymes involved in the conversion of cellular energy or in the production of biomass rely on the availability of substrates such as molecular hydrogen, oxygen, or carbon dioxide. Examples include cytochrome c oxidase, which catalyzes the 4-electron reduction of O_2 to water,[3,4] hydrogenases, which catalyze the oxidation and production of H_2,[5,6] and carbon monoxide dehydrogenase/acetyl-CoA synthase, which catalyzes the fixation of CO_2 and the first step in the production of biomass.[7,8] Before these reactions can occur, a small molecule of not more than ∼0.3 nm in size must diffuse from the solvent into the enzyme active site, through several nanometers of a heterogeneous protein matrix, typically more densely packed than organic solids.[9] As their solubility in aqueous media is low, gas molecules are a limited resource for enzymes. Moreover, not all gas molecules that are present in solution should access the active site, preferably only the substrate molecule, and not potential inhibitor gases. Thus, efficient and selective transport of gas molecules is a critical issue in enzymatic catalysis.

Experimentally, studies of xenon binding to protein crystals and measurements of gas diffusion rates have given valuable insight into small molecule transport in proteins. For [NiFe]-hydrogenase, on which we focus in this work, a single "VA"-shaped set of gas channels has been identified, extending several nanometers from the active site to the protein surface.[10,11] Its existence led to the assumption that it is the only transport path for the substrate H_2 and for the inhibitors O_2 and CO. Moreover, two residues, Val74 and Leu122, located at one end of the channel in close proximity to the active site, were hypothesized to act as a "gate", controlling the access of gas molecules to the active site. In a recent series of elegant mutation experiments, the function of these two residues was investigated.[12−14] They were mutated into bulkier amino acids, and the rate of CO diffusion into the active site was measured using a novel protein film voltammetry technique.[12] A significant decrease in the diffusion rate was found for mutations involving Val74, suggesting that the larger residues narrowed the proposed channel. However, it was unclear why none of the Leu122 single mutants had any significant effect.

On the theoretical side, molecular dynamics simulations have generated useful information about likely gas transport pathways in a wide range of proteins, including myoglobin[15−24] (reviewed in ref 1), flavin-containing mono-oxygenase[25] and oxidases[25−27] (reviewed in ref 2), carbon monoxide dehydrogenase/acetyl-CoA synthase,[8] nitrogenases,[28] copper amino oxidase,[29] lipoxygenase,[30]

Received: October 28, 2010
Published: February 22, 2011

and hydrogenases.[10,31−33] Specifically, for [FeFe]-hydrogenase, it was suggested that H_2 can easily migrate through a series of static cavities to the outside of the protein, whereas for O_2 protein dynamical motions play a role in facilitating diffusion into the solvent.[31,32] Simulations of [NiFe]-hydrogenase showed that H_2 can diffuse from the solvent to the active site within less than 10 ns, and that Val67 may be a control point for gas access to the active site.[33] These previous simulations gave interesting qualitative insights into gas diffusion in hydrogenases. However, they did not yield quantitative properties such as diffusion rates, that could be compared to experimental rate measurements.

The ability to compute diffusion rates and pathways would greatly enhance our microscopic understanding of gas transport in proteins. Experimental rate measurements could be given a molecular interpretation, and computational predictions of the effect of mutations on the diffusion rate could be made. Moreover, one could use the comparison with the experimental data to assess the quality of the molecular simulations on which the mechanistic interpretations are based. Rate calculations have not been carried out before for hydrogenase because an underlying theoretical model was missing. Thus, with the recent development of two experimental methods for probing the rates of diffusion in hydrogenases, it is very timely to develop such a theoretical approach.

Here, we describe gas diffusion in very general terms, as a Markov process, in which the gas molecules make transitions between discrete sites in the enzyme, identified by molecular simulation. Using data from equilibrium and nonequilibrium simulations in the presence of a pulling force, we estimate the rates for these transitions and solve a coarse master equation to obtain time-dependent populations. We find that the population of the active site follows an effective monoexponential curve in agreement with a phenomenological description for gas diffusion. This correspondence allows us to relate the microscopic overall rate with the experimentally determined diffusion rate. The numerical values obtained are in very good agreement with experiment. However, in contrast to the single pathway picture proposed previously, we identify three distinct pathways for gas diffusion, each terminating in a single cavity from which gas molecules make the final transit into the active site pocket. In light of the present calculations, we propose an alternative explanation for the strong decrease in the diffusive CO on-rates reported in recent mutation experiments.[14] We also argue that the Val74−Arg476 rather than the Val74−Leu122 motif could be key to the engineering of a molecular sieve selective for O_2.

2. METHODOLOGY

2.1. Theory. *2.1.1. Coarse Master Equation.* To motivate our theoretical model for the calculation of gas diffusion rates in proteins, we consider a typical molecular dynamics trajectory of a gas molecule in the protein interior as depicted in Figure 1 for [NiFe]-hydrogenase. The trajectory is colored from blue to gray to brown to red to indicate the increasing simulation time. We observe that the gas (H_2) enters the protein and moves via diffusive jumps between protein cavities toward the [NiFe] active site. A similar diffusive behavior of gas molecules has been reported before.[10,32,33] It suggests that the dynamics can be treated as Markovian hopping between these sites, assuming that "memory" is lost within the residence time in any of the cavities. Thus, we coarse grain the diffusive dynamics of the gas molecules in the protein and solvent using a Markovian model. Each gas

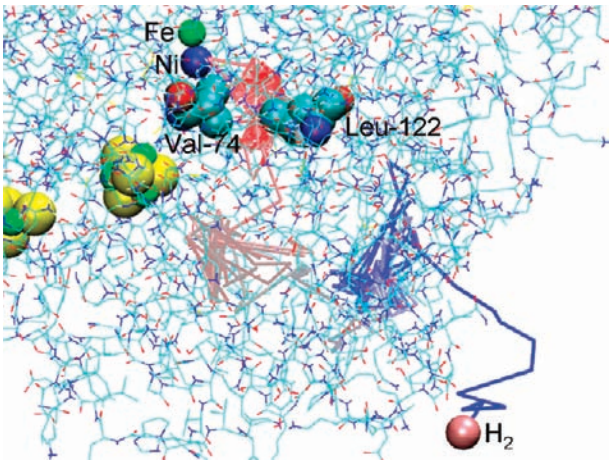

Figure 1. Trajectory of a H_2 molecule inside [NiFe]-hydrogenase as obtained from molecular dynamics simulation at 300 K. The trajectory is colored blue to gray to brown to red for increasing simulation time. The gas molecule is placed in the solvent at the beginning of the run. It enters the protein and moves toward the [NiFe]-active site by diffusive "jumps". The protein is represented as sticks, the [NiFe]-active site, the residues Val74 and Leu122, and the FeS clusters as spheres. Color code: Fe, light green; Ni, blue; S, yellow; O, red; C, dark green. The blue sphere of Leu122 denotes a N atom.

molecule is assumed to reside either in a discrete site within the protein (also called a "cluster" or "state" and denoted by i or j in the following) or in the solvent. The dynamics between these states can then be approximated by a master equation:[34,35]

$$\dot{p}_i(t) = \sum_j k_{ij} p_j(t) \tag{1}$$

where the k_{ij} are the rate constants for the transitions $i \leftarrow j$, representing the constant elements of the rate matrix **K**, and p_i is the population of state i. The rate matrix satisfies three conditions:

$$k_{ij} \geqslant 0 \quad \forall i \neq j \tag{2}$$

$$k_{ii} < 0 \quad \forall i \tag{3}$$

$$\sum_i k_{ij} \equiv 0 \tag{4}$$

Equation 1 can be solved formally in terms of a matrix exponential:

$$p_i(t) = \sum_j (e^{t\mathbf{K}})_{ij} p_j(0) \tag{5}$$

which can be used to calculate the time-dependent population of the cavities from a given initial state.

Here, we are specifically interested in the kinetics of gas diffusion from the solvent to the protein active site, which we denote in the following as site G (for "geminate" state). In this case, we start from an initial state in which the entire population of gas molecules is located in the solvent, as would be the case in experiment, and calculate the time-dependent population of site G, $p_G(t)$, using eq 5.

2.1.2. Phenomenological Rate Model. In the second step, we relate $p_G(t)$ to the rate constants of a phenomenological model for gas diffusion. This will give the computed phenomenological rate constant for gas diffusion from the solvent to the active site cluster G, that can be readily compared to the experimental

dx.doi.org/10.1021/ja109712q | J. Am. Chem. Soc. 2011, 133, 3548–3556

diffusion rate. For hydrogenase, the association reaction between the free enzyme (enz) and gas molecules (gas) has been described in terms of a two-step kinetic scheme:[14]

$$\mathrm{enz} + \mathrm{gas} \underset{k_{-1}}{\overset{k_{+1}[\mathrm{gas}]}{\rightleftharpoons}} \mathrm{G} \underset{k_{-2}}{\overset{k_{+2}}{\rightleftharpoons}} \mathrm{enz{-}gas} \quad (6)$$

The first step describes the diffusion of the gas into the active site of enz, represented in the current calculations by the state where the gas molecule occupies cluster G. The corresponding diffusion rates are k_{+1} and k_{-1}, respectively. The second step, occurring with forward and reverse rates k_{+2} and k_{-2}, results in the chemical binding of the gas molecule to the active site (enz−gas). Using a classical force field, this second step is not represented in the present calculations. This means that the computed population $p_G(t)$ is only due to the kinetics of the first reaction step. Hence, k_{+2} and k_{-2} can be set equal to zero in the kinetic model for $p_G(t)$. Assuming that the rate matrix **K** in eq 5 has been constructed for constant gas concentration (see section 2.1.3 for details), the population of the geminate cluster is given by the following pseudo-first-order kinetic equation:

$$p_G(t) = \frac{k_{+1}[\mathrm{gas}]}{k_{+1}[\mathrm{gas}] + k_{-1}}[1 - \exp(-(k_{+1}[\mathrm{gas}] + k_{-1})t)] \quad (7)$$

Thus, a fit of $p_G(t)$ to eq 7 gives the desired phenomenological rate for diffusion from the solvent to cluster G, k_1, and the rate for the reverse process, k_{-1}.

2.1.3. Construction of Microscopic Rate Matrix. In the following, we describe the computation of the matrix elements k_{ij} of the rate matrix **K** (eq 1). To construct the rate matrix from the equilibrium simulation, we assume that the simulations are sufficiently long that all relevant transitions have been observed on the simulation time scale. We first construct a transition matrix **N** containing the total number of transitions between each pair of states in the simulations, summed over all gas molecules, where N_{ij} is the number of transitions from j to i. We enforce detailed balance by symmetrizing the matrix of transitions, $N_{ij}^{\mathrm{sym}} = N_{ij} + N_{ji}$. The "branching probability" for the transition from j to i, that is, the probability that the system will make a transition first to i rather than to some other state, is calculated as $N_{ij}^{\mathrm{sym}}/\sum_{l=1}^{N} N_{lj}^{\mathrm{sym}}$. The transition rate from j to i is then given by:[36]

$$k_{ij} = \frac{N_{ij}^{\mathrm{sym}}}{T_j \sum_{l=1}^{N} N_{lj}^{\mathrm{sym}}}, \quad \forall j \neq i \quad (8)$$

$$k_{jj} = -T_j^{-1} = -\sum_{i=1(i\neq j)}^{N} k_{ij}, \quad \forall j \quad (9)$$

where T_j is the average residence time of a gas molecule in state j and is measured by averaging all times of visiting state j.

While transitions between clusters within the protein are unimolecular, those from the solvent to protein clusters are bimolecular events, so the corresponding microscopic rates depend on gas concentration. Here, we assume that the concentration of gas molecules in the solvent remains constant, which is consistent with experimental conditions for which diffusion rates are measured.[12,14] Consequently, all solvent to protein cluster transitions become unimolecular (i.e., pseudo-first-order in the protein concentration), and the rate matrix described above can be solved in the usual way. However, because the transition rates are calculated from the average residence time of a single gas molecule, the rate matrix constructed from the simulation data is for a gas concentration $1/V_{\mathrm{H_2O}}^{\mathrm{sim}}$, where $V_{\mathrm{H_2O}}^{\mathrm{sim}}$ is the volume of the simulation box outside the protein. To obtain the rate matrix for a reference (e.g., experimental) gas concentration $[\mathrm{gas}]^\circ$, we scale all pseudo-first-order solvent-to-protein rates by a factor $V_{\mathrm{H_2O}}^{\mathrm{sim}}/V_{\mathrm{H_2O}}^{\circ}$, where $V_{\mathrm{H_2O}}^{\circ}$ is the volume per molecule of gas at a gas concentration $[\mathrm{gas}]^\circ$.

2.1.4. Theory of Force-Induced Transitions. Rates for transitions that are not adequately sampled on the time scale of the equilibrium simulations are obtained from nonequilibrium simulations in the presence of a pulling force. The molecule is pulled from the initial (j) to the final cluster (i) for a series of external forces of constant magnitude F. Averaging over initial conditions, the simulations yield the force-dependent mean first passage time (MFPT), $\tau_{ij}(F)$. We use a one-dimensional model for force-dependent kinetics,[37] derived from Kramers theory,[38] to extrapolate the transition rate constant from our pulling simulations to zero force. The Dudko−Hummer−Szabo (DHS) model gives the dependence of the transition rate constant $k_{ij}(F) = 1/\tau_{ij}(F)$ on force F as

$$k_{ij}(F) = k_{ij}^0 \left(1 - \frac{\nu F x^{\ddagger}}{\Delta G^{\ddagger}}\right)^{1/\nu - 1} e^{\Delta G^{\ddagger}[1 - (1 - (\nu F x^{\ddagger}/\Delta G^{\ddagger}))^{1/\nu}]} \quad (10)$$

where $k_{ij}^0 = k_{ij}(0)$ is the rate at zero force, which is equal to the desired rate matrix element k_{ij}, $\Delta G^{\ddagger}$ is the height of the barrier, and $x^{\ddagger}$ is the distance to the transition state. The parameter ν was set equal to 2/3 corresponding to a linear cubic form of the energy surface. This model is able to account for the dependence of the transition state location on force and thus explains the curvature in the force dependence of the kinetics.

2.2. Simulation Details. *Molecular Models.* We have employed the same molecular models for the protein, solvent, and H_2 that were used in a previous study on a homologous [NiFe]-hydrogenase.[33] The GROMOS96 43a1 protein force field[39] and the SPC/E model for liquid water[40] were used. The gas molecules were described by a three-site model comprised of two "real" atoms and a virtual interaction site located at the center of geometry. The two atoms carry charges only so as to reproduce the experimental quadrupole moment, and the virtual site carries Lennard-Jones parameters, only. For H_2, the parametrization of ref 41 was used. For O_2, Lennard-Jones parameters were taken from ref 42 and point charges to reproduce the experimental quadrupole moment of gas-phase O_2. The gas models reproduce the experimental diffusion constant of H_2 and O_2 in water very well, to within a relative error of 7%. In *n*-hexane, the relative error is larger, 43%. This accuracy is still acceptable for the purpose of this investigation, which is the prediction of the correct order of magnitude of the diffusion rate in the enzyme. (Note that experimental measurements of diffusion rates in proteins can have a similar uncertainty.[12,14])

Equilibrium Molecular Dynamics Simulations. The initial configuration of *Desulfovibrio fructosovorans* [NiFe]-hydrogenase was taken from the crystal structure PDB id: 1YQW.[43] The protein was solvated and equilibrated for 10 ns in the NPT

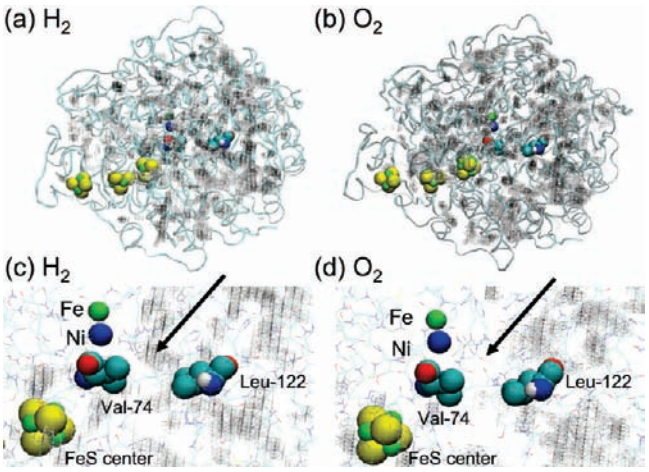

Figure 2. (a) Probability density map for H_2. Probabilities were calculated over the last 40 ns of the 50 ns trajectory, using a 1 Å grid. Grid points are displayed only if they were visited by H_2 molecules inside the protein on at least three separate occasions and are shaded by probability of occupancy on a log scale from gray (low) to black (high). (b) Probability density map for O_2, as in (a). (c) Enlarged view of the map for H_2 near the active site region, with important residues labeled. (d) The corresponding magnified map for O_2. The major difference between H_2 and O_2 maps, indicated by arrows, is the absence of any O_2 from the active site. The color code is the same as in Figure 1.

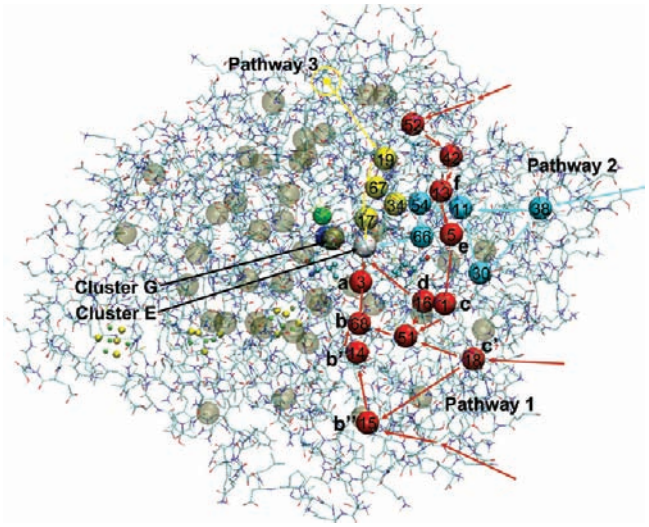

Figure 3. Coarse-graining of hydrogen trajectories inside the enzyme. Motivated by the diffusive hopping of H_2 molecules between cavities in the protein (see Figure 1), we define clusters centered at the regions of high gas density inside the protein. The clusters are depicted as spheres together with three typical "pathways" to the active site observed by following the trajectories (pathways 1, 2, and 3, colored in red, blue, and yellow, respectively). The symbol ⊙ in pathway 3 indicates entry of H_2 molecules from the back of the protein. Cluster E in white is the cluster that gas molecules temporally occupy before binding, with cluster G in gray the final state when a gas molecule is able to bind Ni. The labels a, b, etc., denote the approximate positions of the Xe-peaks reported in ref 10. The important residues, including Val74, Leu122, and FeS cluster, are shown as spheres. The color code is the same as in Figure 1.

ensemble at 300 K and 1 bar (average secondary structure root-mean-square deviation (rmsd) = 1.66 Å with respect to crystal structure). Simulations including the gases were carried out similarly to those in ref 33. The runs were initiated from the final configuration of the protein only run, by randomly replacing 100 water molecules by H_2 or O_2 molecules outside the protein. A 50 ns NPT simulation was run for each system. The gas concentration in our simulation is 225 mM, corresponding to roughly 200−300 times higher than the saturated concentration under a pressure of 1 atm gas. We have chosen this relatively high concentration to obtain improved statistics for simulation of the diffusion process. The total system comprising the protein and solvent is large enough, however, so that interactions between gas molecules can be assumed to have a negligible effect on the dynamics of gas diffusion. The protein is stable over the course of the simulation, reaching an average secondary structure rmsd of 1.83 Å with respect to crystal structure.

Assignment of States in Configuration Space. To define states for our Markov model,[44] we clustered the interior densities of H_2 molecules as obtained from equilibrium simulation (shown in Figure 2) using the GROMOS algorithm,[45] with a cutoff radius of 6 Å. Although we obtained hundreds of clusters of various sizes, for simplicity we chose 68 clusters (shown in Figure 3), which account for almost all H_2 molecules within the protein. All interior H_2 are assigned to clusters as described below. We defined two clusters in addition to those identified by the automated clustering: the first corresponds to gas molecules in the solvent, defined as regions with zero density of protein atoms, and the second, labeled "G", corresponds to the likely binding site of the gas to the Ni atom in the active site pocket before chemical bond formation. Because H_2 is smaller than O_2 and explores a larger fraction of the protein interior, we assume that the clusters obtained for H_2 include all relevant cavities for O_2. Thus, for O_2, the same definition of clusters was used as for H_2.

Calculation of Transition Rates. Rates for transitions between the states defined above are calculated according to eqs 8 and 9 using the last 40 ns of the 50 ns equilibrium simulations. A major difficulty we encountered with this approach are the apparent "recrossings" caused by the imperfectly drawn boundaries of the stable states.[36,46] Drawing on ideas from transition-path sampling[47,48] and milestoning,[49,50] we define "core" regions for each cluster, for which there is no doubt about the assignment. A trajectory crossing out of one of these regions is only deemed to have made a transition to another cluster when it enters the "core" region of the new cluster; in this way, we avoid apparent transitions when the gas molecules cross approximately drawn state boundaries, but in fact remain in the original metastable state. The "core" region for each cluster i was defined using a spherical radius, of $\lambda d_{\min}(i)$, where $d_{\min}(i)$ is the nearest neighbor distance of i and $\lambda = 0.4$.

Nonequilibrium Pulling Simulations. Rates for the transitions of O_2 molecules from E←14, E←16, E←66, and G←E were estimated from pulling simulations. A series of runs was carried out, applying different sets of external forces $\vec{F}$ of constant magnitude $F = |\vec{F}|$, pointing along the direction between the center of mass of the gas molecule and the destination cluster. The latter was defined as the center of mass of selected atoms in the protein. Each system contained one hydrogenase and one gas molecule; a reduced system was used to accelerate the dynamics (see Supporting Information). The starting point for each simulation was a snapshot from the 50 ns equilibrium simulation in which the gas molecule was in the desired initial cluster. The MFPT ($\tau_{ij}(F)$) was calculated as the average time a gas molecule takes to reach the center of the destination cluster up to a distance of 0.3 Å. For each force, between 51 and 200 replicates with the same configuration were

dx.doi.org/10.1021/ja109712q | J. Am. Chem. Soc. 2011, 133, 3548–3556

run using different initial velocities generated from a Maxwell distribution at a temperature of 300 K. The force-dependent MFPTs were fit to the inverse of eq 10 (using $\tau_{ij}(F) = 1/k_{ij}(F)$) and the MFPT at zero force, τ_{ij}°, obtained from extrapolation. The latter was converted to the desired rate, $k_{ij}^{\circ} = 1/\tau_{ij}^{\circ}$, and inserted into the rate matrix **K**. We have validated this approach by carrying out a pulling simulation for H_2 (E←14) and found that τ_{ij}° obtained from zero force extrapolation was in good agreement with the MFPT obtained from equilibrium simulation. The reverse rates for transitions for which pulling simulations were carried out, k_{ji}, were obtained from the equilibrium constant $K_{ij} = k_{ij}/k_{ji}$. It was assumed that K_{ij} for O_2 is the same as the one for H_2, with the latter estimated from equilibrium simulation. This assumption is justified when gas-specific interactions are absent, so that K_{ij} is mainly determined by the difference in the gas-accessible volume of clusters i and j.

3. RESULTS

3.1. Gas Equilibrium Distributions. We start with a long molecular dynamics simulation of two systems, one containing an equilibrated aqueous solution of hydrogenase and 100 H_2 molecules initially placed in the solvent, and the other containing 100 O_2 molecules instead of H_2 (see section 2.2 for simulation details). We find that both gases quickly permeate the protein, reaching a stable partition between solvent and protein after about 10 ns of simulation time (Figure S1 in the Supporting Information). The partition coefficient, $K_p = [\text{gas}]_p/[\text{gas}]_s$, where $[\text{gas}]_p$ and $[\text{gas}]_s$ are the gas concentrations in the protein and solvent phase, respectively, is larger than 1 for both gases, $K_p = 1.7$ for H_2 and 2.8 for O_2. Thus, H_2 and particularly O_2 favor the protein phase over the solvent. The probability maps shown in Figure 2 reveal that both gases can occupy sites distributed throughout the protein. The regions colored black correspond to probability peaks. The local concentration of gas molecules at these sites is higher than in the solvent by more than K_p, because this parameter refers to the average concentration in the protein. Thus, our numerical data support previous suggestions that internal cavities function as gas reservoirs,[5] although the probability maxima are scattered throughout the protein and are not restricted to the functional gas tunnels (see section 3.2).

Analyzing the probability map in more detail, we find that H_2 can approach the active site up to a distance of 3.1 Å from the Ni atom during the 50 ns simulation. The map near the active site is shown magnified in Figure 2c. These graphs helped us identify the H_2 molecules that have entered the active site vicinity during the simulation (marked by an arrow in Figure 2c). In total, we observed 14 separate events in which H_2 entered the active site vicinity within 50 ns. On the same simulation time scale, only two O_2 molecules were found to visit the active site vicinity, as is indicated by the vanishing probability density, marked by an arrow in Figure 2d. The probability densities for both H_2 and O_2 in Figure 2 suggest that it would be difficult to construct a description of gas entry based on a well-defined "pathway", at least not a priori. Clearly, a more general model that does not rely on preselected pathways is necessary, such as the coarse grained Markovian hopping model described in section 2.1.1.

3.2. Diffusion Paths. The probability density of H_2 was used to define the states of our Markov model by application of a clustering algorithm (see section 2.2 for details). The clusters obtained are depicted as spheres in Figure 3. They correspond to regions of high gas molecule density. We find that the clusters are scattered throughout the protein and account for 95% of the population of H_2 molecules within the protein. All previously reported Xe-peaks[10] (denoted by labels a, b, etc., in Figure 3) could be assigned to clusters except peak e′. The latter is combined with one of the other clusters and not identified as a separate site by our clustering algorithm. The automatically identified cluster closest to the active site, denoted cluster E, is about 7 Å away from the Ni atom and corresponds to the active site vicinity that was visited by H_2 14 times as described in Section 3.1. On the basis of the closest approach of a single hydrogen molecule to the active site, we have defined an additional cluster denoted "G", which corresponds to the likely binding site of the gas to the Ni atom in the active site pocket before chemical bond formation takes place. Cluster G, first introduced in Section 2.1, is about 3 Å away from the Ni site and can be regarded as the "geminate" state described by Liebgott et al.[14]

We find that the gas molecules that reach cluster G do so via transition from cluster E, only. Tracing back the trajectories of the 14 H_2 molecules that reached cluster E, we identified three qualitatively distinct "pathways". They can be described by a string of clusters connecting E with the solvent, as indicated in Figure 3. Pathway 1 shown in red resembles the "VA"-shaped set of tunnels first identified in ref 10. We observed that the gas can enter this pathway at four sites, cluster 15 corresponding to Xe-peak b″ in ref 10, cluster 18 corresponding to peak c′, cluster 16 corresponding to peak d, and cluster 52 corresponding to the path adjacent to peak e′. No entry of gas molecules was observed near peak f. All gas molecules that enter the protein through clusters 15, 18, and 52 reach the active site vicinity (cluster E) from "below" and have to cross the Val74—Leu122 motif at the end of the tunnel.

Our simulations show that there are at least two more routes that gas molecules can take to reach cluster E. The second pathway shown in turquoise starts on the same side of the protein as pathway 1, but leads more directly into the active site vicinity. This pathway is not part of the "VA"-shaped set of tunnels because the gas molecules that follow this route enter the active site vicinity "sideways", that is, orthogonal to pathway 1, and they do not cross the Val74—Leu122 passage before they enter the active site. A third pathway shown in yellow starts on the back side of the protein and enters the active site vicinity from "above", opposite to pathway 1. Also, on this route, gas molecules do not cross the Val74—Leu122 motif. It is worth mentioning that pathways 1 and 2 are surrounded predominantly by hydrophobic residues and pathway 3 by hydrophobic and hydrophilic residues. As a consequence, the population of water molecules in the cavities that form the three pathways is in general low, even though there is a significant interior water density in certain regions of the protein.

3.3. Diffusion Rates. To compute gas diffusion rates, we use the coarse-grained states defined above to build a master equation for the gas dynamics according to eq 1. For H_2, it is possible to construct the full rate matrix **K** from equilibrium simulations alone via eqs 8 and 9. Also for O_2 most of the transitions could be estimated from equilibrium runs, except the transition into cluster E, which was observed only rarely, and the transition from E to G, which was not observed at all during the 50 ns equilibrium simulation (longer simulation times would have been necessary to observe also this transition, although at a prohibitive computational cost).

To estimate the rates for transitions into E and G, we have used the nonequilibrium pulling simulation as described in section 2.1.4. Within pathway 1, we chose the transitions E←14 and E←16. We based this choice on the observation that O_2 made

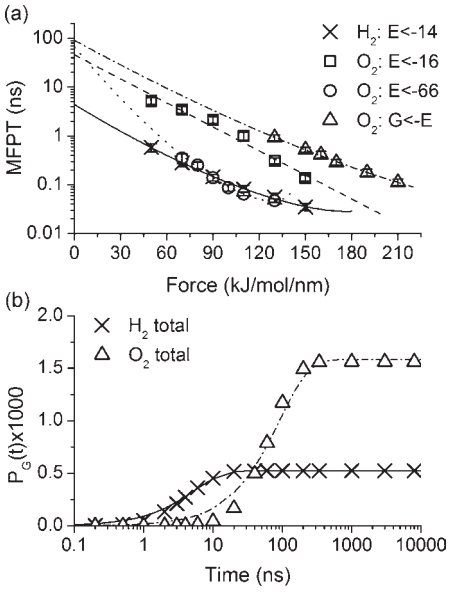

Figure 4. (a) Mean first passage time (MFPT) as obtained from constant-force pulling for transitions between clusters as indicated. See Figure 3 for the position of the clusters in the protein. Data points were fit to the inverse of eq 10, and the fits were used to calculate the MFPT at zero force. (b) Gas population probability of the active site cluster G as a function of time. Data points were obtained by solving the master equation according to eq 5 starting from initial conditions ($t = 0$) where the entire population of gas molecules is located in the solvent. For O_2, the rate matrix was constructed from equilibrium and pulling simulations (shown in pannel a), and for H_2, only equilibrium simulation data were used. The data points were fit to the phenomenological rate equation (eq 7).

two transits E←16 during the equilibrium simulation, and that E←14 was the dominant transition for H_2 molecules into E. All other transitions from clusters of pathway 1 into E are expected to have a significantly lower transition rate and are thus neglected. Within pathway 2, we have chosen the transition E←66 because this was the only feasible transition for H_2. Again, we expect that all other transitions into E are significantly less favorable. We also carried out pulling simulations for the transition G←E. This is the only transition by which gas molecules can reach the active site. No pulling simulations were carried out for transitions between clusters of pathway 3 and cluster E because this pathway contributes least to the total H_2 flux.

The results of the pulling simulations are summarized in Figure 4. In panel a, the mean first passage time (MFPT) τ_{ij} is shown as a function of the pulling force for some of the transitions described above. The MFPT is the average time it takes for a gas molecule in cluster j to make a transition to i. The data points fit the Dudko−Hummer−Szabo model for force-dependent kinetics[37] very well (inverse of eq 10), with correlation coefficients between 0.97(E←16, O_2) and 0.998 (G←E, O_2). This model is able to account for the dependence of the transition state location on force and thus explains the curvature in the force dependence of the kinetics for the transitions E←66 (O_2) and E←14 (H_2, this pulling simulation was carried out for validation purposes only). The desired transition rate k_{ij} is equal to the inverse of the MFPT extrapolated to zero force. For O_2, these rates are then inserted into the rate matrix **K**.

Starting from an initial state in which the entire population of gas molecules is located in the solvent S ($p_S(t = 0) = 1$, $p_k(t = 0) = 0$ for all $k \neq S$) as would be the case in the experiment, we calculated the time evolution of the cluster populations by solving the master equation, eq 5. The time-dependent probability of finding a gas molecule in the active site cluster G, $p_G(t)$, is illustrated in Figure 4b. We find that for H_2 as well as for O_2, $p_G(t)$ is characteristic of an effective first-order kinetic process. Most importantly, we find that $p_G(t)$ fits very well the phenomenological rate equation derived in section 2.1.2, eq 7 (best fits indicated in solid lines). The phenomenological rate constants k_{+1} and k_{-1} extracted from the fits are summarized in Table 1.

Table 1. Computed (comp) Rates for Diffusion of H_2 and O_2 from the Solvent to the [NiFe]-Hydrogenase Active Site, k_{+1}, for Diffusion Out of the Active Site, k_{-1}, and the Experimentally (exp) Determined On-Rate for CO, k_{in}

	H_2 (comp)		O_2 (comp)		CO (exp)
	k_{+1}[a]	k_{-1}[b]	k_{+1}[a]	k_{-1}[b]	k_{in}[c]
total	9.9 (6.6)	1.9 (0.3)	**1.7** (0.6)	0.11 (0.03)	**1−2**
blocked[d]	7.7 (1.4)	1.2 (0.3)	0.5 (0.2)	0.09 (0.02)	

[a] In units $10^4\ s^{-1}\ mM^{-1}$. [b] In units $10^8\ s^{-1}$. [c] In units $10^4\ s^{-1}\ atm(CO)^{-1}$, ref 12. Note that the difference between $s^{-1}\ atm(CO)^{-1}$ and $s^{-1}\ mM^{-1}$ is negligibly small. [d] Pathway 1 blocked.

We find that the computed rate for O_2 diffusion into G, $k_{+1}^{O_2} = (1.7 \pm 0.6) \times 10^4\ s^{-1}\ mM^{-1}$, is within the range of experimental values for the CO on-rate k_{in}^{CO} (figures in bold in Table 1). Unfortunately, experimental values for $k_{+1}^{O_2}$ are not available, because the measured $k_{in}^{O_2}$ for reaction eq 6 is limited by k_{+2}. However, because of its similar size and mass, it can be assumed that the diffusion rate of O_2 into the active site is very similar to the one of CO. Indeed, recent mutation experiments were consistent with the assumption that the on-rate for CO is a good proxy for the O_2 diffusion rate into the active site, that is, $k_{+1}^{O_2} \approx k_{+1}^{CO} \approx k_{in}^{CO}$.[14] In a separate investigation that will be described in detail in a forthcoming publication, we have also computed the diffusion rate of CO molecules into the hydrogenase active site. The value obtained, $k_{+1}^{CO} = (1.1 \pm 0.4) \times 10^4\ s^{-1}\ mM^{-1}$, is only marginally smaller than for O_2, confirming the above relation. The good agreement between computed and experimental rates strongly supports our theoretical model for gas transport in the hydrogenase enzyme.

An interesting question concerns the difference in the diffusivity of H_2 and O_2. Given the difference in size and mass, it should not be surprising that H_2 diffuses faster into the active site than O_2. Indeed, our calculation gives a diffusion rate for H_2 that is a factor of about 6 larger than for O_2 (k_{+1} in Table 1). For comparison, the diffusion coefficients of H_2 in water and *n*-hexane are only a factor of 2.1 and 1.7 higher than for O_2. Thus, our calculations predict that native hydrogenase exhibits an about 3-fold higher selectivity in favor of H_2 than typical polar and nonpolar liquids.

3.4. Reactive Flux Analysis. To place our analysis of the accessible pathways on a more quantitative basis, we have used a recently developed formalism for calculating contributions to the reactive flux from kinetic master equations.[51] We divide our clusters into two end states, S and G corresponding to the solvent and cluster G, respectively, and a transition region I consisting of all the other clusters inside the protein. The first step of the calculation is to determine the committor, $\phi_G(x)$, for each cluster x, defined as the probability that a trajectory initiated from x will reach G before reaching S: by definition, $\phi_G(G) = 1$ and $\phi_G(S) = 0$. The remaining committors can be self-consistently determined

dx.doi.org/10.1021/ja109712q | J. Am. Chem. Soc. 2011, 133, 3548–3556

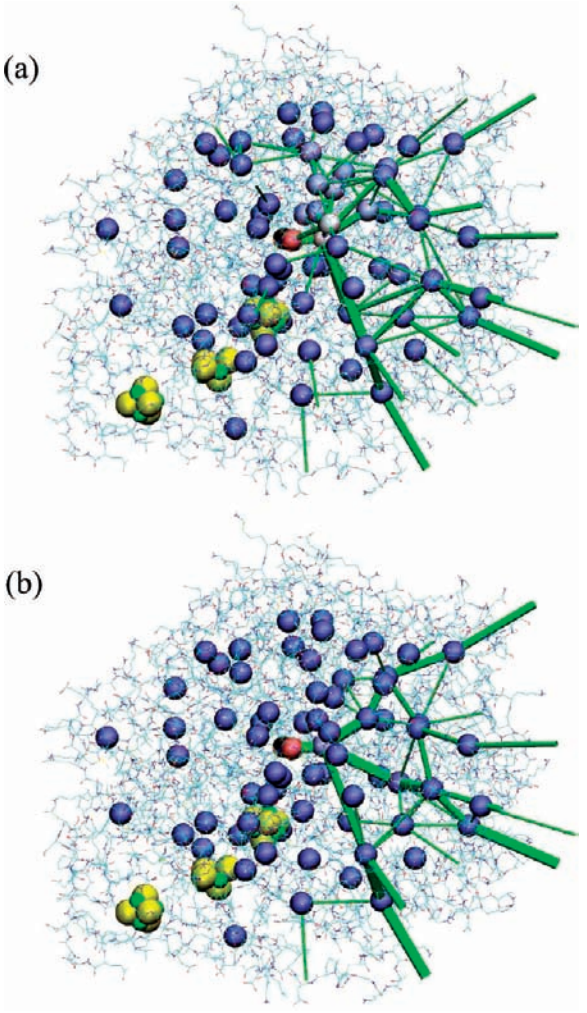

Figure 5. Reactive flux toward the active site. The flux of gas molecules reaching the active site is calculated for each transition in the network, as a fraction of the total for (a) H_2 and (b) O_2. The cross-sectional area of each connection is approximately proportional to the flux along it, and the committor for each cluster x, $\phi_G(x)$ (see text), is indicated using a color scale from blue for $\phi_G(x) = 0$ through white to red for $\phi_G(x) = 1$.

from these boundary conditions (see Supporting Information). We calculate the contribution to the total reactive flux $J_{i\to j}$ for a given transition between clusters i and j, the fraction of the reactive flux coming from trajectories, which traverse the edge $i\to j$, as $J_{i\to j} = K_{ji}p_{eq}(i)[\phi_G(j) - \phi_G(i)]$, for $\phi_G(j) > \phi_G(i)$.[51]

The results are shown in Figure 5. The committors reveal that for most clusters, it is more probable that the gas will return to the solvent rather than reach the active site. This is particularly true for oxygen, where the final barriers to reaching the active site are relatively high. The weights of the edges illustrated in the figure indicate the relative flux along each, confirming the qualitative picture inferred from the equilibrium trajectories of hydrogen. About 57% of the H_2 molecules that reach the active site enter the protein at entry points of pathway 1 and diffuse within the main channel toward cluster E. However, there is also some significant contribution due to pathway 2, 26%, with gas entry sideways via cluster 38. A smaller contribution of 17% is due to pathway 3. Our simulations give no evidence that O_2 uses pathways that are significantly different from the ones of H_2. The reactive flux for O_2, shown in Figure 5b, is qualitatively similar to the one for H_2.

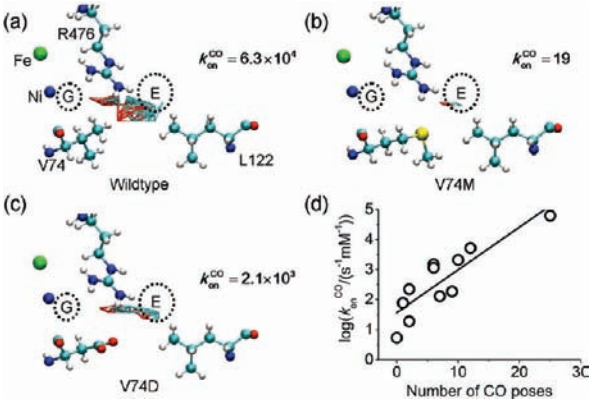

Figure 6. Volume-accessible poses of a CO molecule between clusters E and G for wild-type (WT) [NiFe]-hydrogenase (a), V74 M (b), and V74D mutants (c). The CO molecule is represented in stick representation, and key residues are depicted in ball and stick representation. The color code is the same as in Figure 1. In the WT, V74D, and V74M mutants, there are 25, 10, and 2 possible poses, respectively. The experimentally determined on-rate for CO binding,[14] k_{+1}^{CO}, is given in units s^{-1} mM^{-1}. In panel (d), the number of CO poses determined for WT and 10 mutants is plotted against the experimentally determined on-rate[14] (○). The best linear fit is shown in solid lines.

4. DISCUSSION

Previous analyses of Xe-binding sites have led to the picture that gas diffusion in [NiFe]-hydrogenase occurs through a set of gas channels that facilitate transport as depicted by pathway 1 of Figure 3. Our present simulations suggest that there are at least two additional pathways that gas molecules can take to reach the protein active site, denoted pathways 2 and 3 in Figure 3. These routes have a different entry point at the protein surface, and they follow distinct paths to the active site vicinity. These additional paths were not revealed by the Xe-binding experiments, which probe the most favorable sites for the Xe molecules to reside at equilibrium rather than reflecting the flux of gas molecules toward the active site. Neither did cavity calculations on static crystal structures reveal these paths. This implies that pathways 2 and 3 are dynamically formed and temporary in nature. Interestingly, all three paths terminate at a single cluster, E, about 7 Å away from the Ni site, which is connected with the active site cluster G. A similar "funnel" architecture was recently described for gas diffusion in a mono-oxygenase and an oxidase.[2,25]

The picture of gas diffusion obtained from present simulations sheds new light on recent mutation studies, where a dramatic decrease in the diffusive on-rate for CO was reported when Val74 was mutated into more bulky amino acids.[12−14] It was hypothesized that Val74 and Leu122, located at the end of pathway 1, just before cluster E, act as control points (see Figure 6). The mutations of Val74 would narrow this passage, preventing CO from passing to the active site. This explanation was supported by the crystal structure of the V74M mutant, showing that Met74 and Leu122 are in van der Waals contact, thereby blocking CO diffusion. However, what could not be explained was that mutations of the other residue, Leu122, did not have any effect on the CO on-rate. This is at odds with the hypothesis that the decrease in the on-rate is due to the narrowing of the passage between Val74 and Leu122, because then one would expect that mutation of Leu122 into bulkier amino acids would at least have some effect.

Here, we present a possible alternative explanation of the observed mutation effect. Inspection of the active site pocket of

WT (PDB id: 1YQW)[43] and V74M (PDB id: 3H3X)[13] mutant reveals that the mutation not only narrows the free space between Met74 and Leu122, but also between Met74 and Arg476 (see Figure 6a,b). The latter passage is the final bottleneck for the transition from cluster E to the active site cluster G. We have analyzed this situation in more detail by determining the possible, volume-accessible poses of a CO molecule between clusters E and G for WT, V74M, and all other mutants for which diffusive CO on-rates have been measured.[14] The side chain of mutants for which no crystal structure was available was modeled on the basis of the conformation of the V74M mutant. In this case, the most probable orientation of the side chain was chosen according to a rotamer library.[52] CO poses were enumerated by placing the CO molecule on a 0.5 Å grid and allowing 2016 orientations. A pose was accepted when both atoms of the CO molecule did not overlap with any protein atom (see Supporting Information for further details).

As illustrated in Figure 6a−c for WT, V74M, and V74D, we find that the number of volume-accessible CO poses between clusters E and G (depicted in stick representation) decreases with decreasing on-rate. A plot of these two quantities for WT and the 10 mutants shows a good linear correlation, with a correlation coefficient of 0.87; see Figure 6d and Table S1 for a summary of numerical values. The data support our hypothesis that the decrease in the on-rate could be at least in part due to the narrowing of the free space between Val74 and Arg476. While this may serve as an explanation for why mutations of Leu122 did not have any significant effect on the on-rates, a note of caution is appropriate here. Our analysis with CO as a probe was carried out for static crystal structures and did not include dynamical effects. Thus, computation of transition rates into cluster E and G of the mutants is clearly necessary to further support our proposal. This will be the subject of forthcoming work.

The Val74−Arg476 motif could also play a key role in attempts to block oxygen access to the active site. As we found that O_2 can access the active site via pathways 2 and 3, the narrowing of pathway 1 at the passage Val74−Leu122 would not have much of an effect. Indeed, simulating the blocking of the passage between Val74−Leu122 by setting all transition rates between clusters of pathway 1 and cluster E to zero, we find that the diffusion rate in the active site is reduced by only about 60% for O_2 (20% for H_2, see Table 1 "blocked"). Thus, restriction of O_2 access could possibly only be achieved by narrowing the passage between clusters E and G, that is, by modifying the Val74−Arg476 motif.

We further note that blocking the access to the active site is not the only mechanism by which hydrogenases can acquire oxygen tolerance. Recent experimental work on membrane bound hydrogenases from Knallgas bacteria has shown that the formation of an easily recoverable oxidation product and the rapid reductive reactivation of this state are other crucial factors determining the oxygen tolerance of the enzyme.[53,54]

5. CONCLUSION

We have developed a general approach for the calculation of gas diffusion rates inside proteins. Application to [NiFe]-hydrogenase gave rate constants in good agreement with experiment, showing that our approach can be regarded as a step toward a more quantitative theoretical description of this important physical process in biology, which may be tested further by future applications. Our simulations indicate that the hydrogenase protein structure "funnels" gas molecules from at least a few different possible pathways into a well-defined cavity close to the active site, from which gas molecules can move on to the final binding site. This picture differs from the single tunnel paradigm,[10,12−14] but is supported by the rates computed from the same simulation. Finally, we proposed an alternative explanation for the dramatic decrease in the diffusion rate observed for some mutants. We proposed that the Val74−Arg476 motif could be key to the engineering of a gas filter that blocks the access of O_2 molecules to the active site. Future rate calculations for hydrogenase mutants[14] as well as experimental mutation studies on Arg476 will be helpful to confirm this hypothesis.

■ ASSOCIATED CONTENT

Supporting Information. Details of the MD simulation protocols and of the determination of CO poses, a graph showing the percentage of gas molecules inside the protein versus time, a table summarizing the number of CO poses for each mutant, and the full refs 13 and 14. This material is available free of charge via the Internet at http://pubs.acs.org.

■ AUTHOR INFORMATION

Corresponding Author
rbb24@cam.ac.uk; j.blumberger@ucl.ac.uk

■ ACKNOWLEDGMENT

P.-h.W. acknowledges the Ministry of Education, Republic of China (Taiwan), for a Ph.D. scholarship. R.B.B. and J.B. are supported by Royal Society University Research Fellowships.

■ REFERENCES

(1) Elber, R. *Curr. Opin. Struct. Biol.* **2010**, *20*, 162.
(2) Baron, R.; McCammon, J. A.; Mattevi, A. *Curr. Opin. Struct. Biol.* **2009**, *19*, 672.
(3) Salmonsson, L.; Lee, A.; Gennis, R. B.; Brzezinski, P. *Proc. Natl. Acad. Sci. U.S.A.* **2004**, *101*, 11617.
(4) Kim, Y. C.; Wikström, M.; Hummer, G. *Proc. Natl. Acad. Sci. U.S.A.* **2009**, *106*, 13707.
(5) Fontecilla-Camps, J. C.; Volbeda, A.; Cavazza, C.; Nicolet, Y. *Chem. Rev.* **2007**, *107*, 4273.
(6) Armstrong, F. A.; Belsey, N. A.; Cracknell, J. A.; Goldet, G.; Parkin, A.; Reisner, E.; Vincent, K. A.; Wait, A. F. *Chem. Soc. Rev.* **2009**, *38*, 36.
(7) Doukov, T. I.; Blasiak, L. C.; Seravalli, J.; Ragsdale, S. W.; Drennan, C. L. *Biochemistry* **2008**, *47*, 3474.
(8) Tan, X.; Loke, H.; Fitch, S.; Lindahl, P. *J. Am. Chem. Soc.* **2005**, *127*, 5833.
(9) Harpaz, Y.; Gerstein, M.; Chothia, C. *Structure* **1994**, *2*, 641–649.
(10) Montet, Y.; Amara, P.; Volbeda, A.; Vernede, X.; Hatchikian, E. C.; Field, M. J.; Frey, M.; Fontecilla-Camps, J. C. *Nat. Struct. Biol.* **1997**, *4*, 523.
(11) Ogata, H.; Lubitz, W.; Higuchi, Y. *J. Chem. Soc., Dalton Trans.* **2009**, 7577.
(12) Leroux, F.; Dementin, S.; Burlatt, B.; Cournac, L.; Volbeda, A.; Champ, S.; Martin, L.; Guigliarelli, B.; Bertrand, P.; Fontecilla-Camps, J. C.; Rousset, M.; Leger, C. *Proc. Natl. Acad. Sci. U.S.A.* **2008**, *105*, 11188.
(13) Dementin, S.; et al. *J. Am. Chem. Soc.* **2009**, *131*, 10156.
(14) Liebgott, P.-L.; et al. *Nat. Chem. Biol.* **2009**, *63*, 6.
(15) Elber, R.; Karplus, M. *J. Am. Chem. Soc.* **1990**, *112*, 9161.
(16) Schaad, O.; Zhou, H. X.; Szabo, A.; Eaton, W. A.; Henry, E. R. *Proc. Natl. Acad. Sci. U.S.A.* **1993**, *90*, 9547.

(17) Hummer, G.; Schotte, F.; Anfinrud, P. A. *Proc. Natl. Acad. Sci. U.S.A.* **2004**, *101*, 15330.
(18) Cohen, J.; Arkhipov, A.; Braun, R.; Schulten, K. *Biophys. J.* **2006**, *91*, 1844.
(19) Cohen, J.; Schulten, K. *Biophys. J.* **2007**, *93*, 3591.
(20) Ruscio, J. Z.; Kumar, D.; Shukla, M.; Prisant, M. G.; Murali, T. M.; Onufriev, A. V. *Proc. Natl. Acad. Sci. U.S.A.* **2008**, *105*, 9204.
(21) Nishihara, Y.; Hayashi, S.; Kato, S. *Chem. Phys. Lett.* **2008**, *464*, 220.
(22) Ceccarelli, M.; Anedda, R.; Casu, M.; Ruggerone, P. *Proteins* **2008**, *71*, 1231.
(23) Maragliano, L.; Cottone, G.; Ciccotti, G.; Vanden-Eijnden, E. *J. Am. Chem. Soc.* **2009**, *132*, 1010.
(24) D'Abramo, M.; Di Nola, A.; Amadei, A. *J. Phys. Chem. B* **2009**, *113*, 16346.
(25) Baron, R.; Riley, C.; Chenprakhon, P.; Thotsaporn, K.; Winter, R. T.; Alfieri, A.; Forneris, F.; van Berkel, W. J. H.; Chaiyen, P.; Fraaije, M. W.; Mattevi, A.; McCammon, J. A. *Proc. Natl. Acad. Sci. U.S.A.* **2009**, *106*, 10603.
(26) Piubelli, L.; Pedotti, M.; Molla, G.; Feindler-Boeckh, S.; Ghisla, S.; Pilone, M. S.; Pollegioni, L. *J. Biol. Chem.* **2008**, *283*, 24738.
(27) Chen, L.; Lyubimov, A. Y.; Brammer, L.; Vrielink, A.; Sampson, N. S. *Biochemistry* **2008**, *47*, 5368.
(28) Igarashi, R. Y.; Seefeldt, L. *Crit. Rev. Biochem. Mol. Biol.* **2003**, *38*, 351.
(29) Johnson, B. J.; Cohen, J.; Welford, R. W.; Pearson, A. R.; Schulten, K.; Klinman, J. P.; Wilmot, C. M. *J. Biol. Chem.* **2007**, *282*, 17767.
(30) Saam, J.; Ivanov, I.; Walther, M.; Holzhutter, H. G.; Kuhn, H. *Proc. Natl. Acad. Sci. U.S.A.* **2007**, *104*, 13319.
(31) Cohen, J.; Kim, K.; Posewitz, M.; Ghirardi, M. L.; Schulten, K.; Seibert, M.; King, P. *Biochem. Soc. Trans.* **2005**, *33*, 80.
(32) Cohen, J.; Kim, K.; King, P.; Seibert, M.; Schulten, K. *Structure* **2005**, *13*, 1321.
(33) Teixeira, V. H.; Baptista, A. M.; Soares, C. M. *Biophys. J.* **2006**, *91*, 2035.
(34) Zwanzig, R. *J. Stat. Phys.* **1983**, *30*, 255.
(35) Hummer, G. *New J. Phys.* **2005**, *7*, 34.
(36) Buchete, N.; Hummer, G. *J. Phys. Chem. B* **2008**, *112*, 6057.
(37) Dudko, O. K.; Hummer, G.; Szabo, A. *Phys. Rev. Lett.* **2006**, *96*, 108101.
(38) Kramers, H. *Physica* **1940**, *7*, 284.
(39) Scott, W. R. P.; Hünenberger, P. H.; Tironi, I. G.; Mark, A. E.; Billeter, S. R.; Fennen, J.; Torda, A. E.; Huber, T.; Krüger, P.; van Gunsteren, W. F. *J. Phys. Chem. A* **1999**, *103*, 3596.
(40) Berendsen, H. J. C.; Grigera, J. R.; Straatsma, T. P. *J. Phys. Chem.* **1987**, *91*, 6269.
(41) Hunter, J. E., III; Taylor, D. G.; Strauss, H. L. *J. Chem. Phys.* **1992**, *97*, 50.
(42) Bouanich, J.-P. *J. Quant. Spectrosc. Radiat. Transfer* **1992**, *47*, 243.
(43) Volbeda, A.; Martin, L.; Cavazza, C.; Matho, M.; Faber, B.; Roseboom, W.; Albracht, S.; Garcin, E.; Rousset, M.; Fontecilla-Camps, J. *J. Biol. Inorg. Chem.* **2005**, *10*, 239.
(44) Bowman, G. R.; Beauchamp, K. A.; Boxer, G.; Pande, V. S. *J. Chem. Phys.* **2009**, *131*, 124101.
(45) Daura, X.; Gademann, K.; Jaun, B.; Seebach, D.; van Gunsteren, W.; Mark, A. *Angew. Chem., Int. Ed.* **1999**, *38*, 236.
(46) Sarich, M.; Noé, F.; Schütte, C. *Multiscale Model. Simul.* **2010**, *8*, 1154–1177.
(47) Bolhuis, P. G.; Chandler, D.; Dellago, C.; Geissler, P. L. *Annu. Rev. Phys. Chem.* **2002**, *53*, 291.
(48) Best, R. B.; Hummer, G. *Proc. Natl. Acad. Sci. U.S.A.* **2005**, *102*, 6732–6737.
(49) Faradjian, A.; Elber, R. *J. Chem. Phys.* **2004**, *120*, 10880.
(50) Vanden-Eijnden, E.; Venturoli, M.; Ciccotti, G.; Elber, R. *J. Chem. Phys.* **2008**, *129*, 174102.
(51) Berezhkovskii, A.; Hummer, G.; Szabo, A. *J. Chem. Phys.* **2009**, *130*, 205102.
(52) Lovell, S.; Word, J.; Richardson, J.; Richardson, D. *Proteins* **2000**, *40*, 389.
(53) Ludwig, M.; Cracknell, J. A.; Vincent, K. A.; Armstrong, F. A.; Lenz, O. *J. Biol. Chem.* **2008**, *284*, 465–477.
(54) Cracknell, J. A.; Wait, A. F.; Lenz, O.; Friedrich, B.; Armstrong, F. A. *Proc. Natl. Acad. Sci. U.S.A.* **2009**, *106*, 20681.